Journal of Catalysis **203,** 184–191 (2001)
doi:10.1006/jcat.2001.3295, available online at http://www.idealibrary.com on IDEAL®

On the Structure of Activated Hydrotalcites as Solid Base Catalysts for Liquid-Phase Aldol Condensation

J. C. A. A. Roelofs, D. J. Lensveld, A. J. van Dillen, and K. P. de Jong[1]

Department of Inorganic Chemistry and Catalysis, Debye Institute, Utrecht University, 3508 TB Utrecht, The Netherlands

Received March 20, 2001; revised May 23, 2001; accepted May 29, 2001

Hydrotalcites (HTs) of different, well-defined platelet sizes were hydrothermally synthesized. Activation via calcination and rehydration resulted in highly active catalysts. Their activities in the self-condensation of acetone at 273 K showed a linear increase with the amount of accessible Brønsted basic sites as determined by CO_2 adsorption. The number of accessible sites, based on the CO_2/Al ratio, was below 5%. Both results support our model in which only basic sites near edges of HT platelets are partaking in aldol condensations. Besides incorporation of interlayer OH^- upon rehydration, the hexagonal morphology changed as a result of activation into a more irregular but still layered structure containing mesopores (<10 nm). In contrast to this, HTs with interlayer OH^- prepared via ion exchange preserved their original hexagonal structure, but they lacked the high catalytic activity. The results show an enhanced activity of interlayer OH^- close to disordered edges, obtained via rehydration, in contrast to interlayer OH^- in a regular HT structure.

Key Words: **hydrotalcite; layered double hydroxide; calcination/rehydration; aldol condensation; solid base catalysts.**

INTRODUCTION

In recent years the fine-chemical industry has developed growing interest in the utilization of solid catalysts in base-catalyzed reactions. Replacement of currently used homogeneous alkaline bases by a solid catalyst can result in catalyst reuse and waste stream reduction. Activated hydrotalcites (HTs) are capable of catalyzing liquid-phase aldol condensations at low temperatures. The benzaldehyde–acetone condensation (1) and the condensation reactions of citral with acetone (2) and MEK (3) are examples thereof. An important feature of activated HTs is their high activity at ambient temperatures. Combined with the reported selectivities, HTs are promising catalysts for commercial applications.

The HT structure, $Mg_6Al_2(OH)_{16}CO_3 \cdot 4H_2O$, closely resembles that of brucite, $Mg(OH)_2$. In brucite, magnesium cations are octahedrally coordinated by hydroxyl ions, giving rise to edge-shared layers of octahedra. In HT, part of the Mg^{2+} ions is replaced by Al^{3+} ions, resulting in positively charged cation layers. Charge-balancing anions (usually CO_3^{2-}) and water molecules are situated in the interlayers between the stacked brucite-like cation layers (4–6). The as-synthesized HT structure displays no catalytic activity in aldol condensations.

In general, the applied activation procedure of HT to bring about the catalytic activity consists of two steps. First, a controlled heat treatment to 723–773 K is executed which leads to the formation of an Mg(Al)O mixed oxide phase which is capable of catalyzing various gas-phase condensation reactions (7–12). However, application of calcined HTs in liquid-phase systems at low temperatures has not been very successful (13). In the second activation step the calcined sample is rehydrated at room temperature which results in the restoration of the original layered structure, in which the carbonate ions are replaced by OH^- ions (1–3, 14, 15).

The nature and number of active Brønsted basic sites and the mechanism of the condensation reaction have not been fully elucidated. As a result, the large differences in catalytic activity due to subtle alterations of the activation cannot yet be explained, although in this respect the discussion on the reversibility of the Al coordination is interesting (3, 16–18).

The base-catalyzed self-condensation of acetone yielding diacetone alcohol (DAA), shown in Fig. 1, has been extensively studied by several authors (2, 3, 19–23) and the activated HT catalyst has shown to be highly active and selective at low temperatures. This makes this reaction useful as a model system for fundamental studies on the nature of active sites in HT catalysts.

To study the effects of the calcination/rehydration procedure on the HT structure and activity, HTs provided with interlayer Brønsted sites were also prepared by a procedure which leaves the original layered structure intact. During the past two decades many studies have been undertaken to prepare HTs with a variety of interlayer (expanding) anions. For reviews, see (24) and (25). It has been found that the affinity of HTs for interlayer anions is $CO_3^{2-} \gg SO_4^{2-} \gg OH^- > F^- > Cl^- > Br^- > NO_3^-$ (25, 26).

[1]To whom correspondence should be addressed. Fax: +31 30 2511027. E-mail: k.p.dejong@chem.uu.nl.

0021-9517/01 $35.00

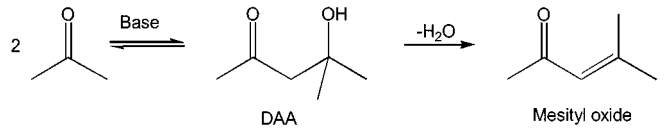

FIG. 1. Base-catalyzed self-condensation of acetone to diacetone alcohol (DAA) followed by dehydration toward mesityl oxide.

Recently, Israëli *et al.* (27) showed that replacement of Cl^- by OH^- is energetically favorable mainly because the latter ion is very similar to interlayer water and forms the best close-packed interlayer arrangement. Kaneyoshi and Jones reported that interlayer terephthalate could be completely exchanged for CO_3^{2-} and SO_4^{2-}, but only partly in the case of NO_3^- and Cl^- (28). We used a HT with the dicarboxylic oxalate ion, prepared according to a procedure reported by Titulaer (30), and replaced this ion by the desired OH^- via ion exchange.

Recently, we reported that only a small number of the OH^- ions in the activated HT are active as Brønsted basic sites in liquid-phase aldol condensations (2). We explained this by assuming that only hydroxyl ions at or near the edges of HT platelets are exposed to the reactants. To test this hypothesis we prepared a series of HTs with different platelet sizes that expose, after activation, different numbers of basic sites per gram. Reichle *et al.* demonstrated that HT platelet sizes can be affected considerably by variation of the aging temperature during synthesis (29). For instance, they obtained crystallites after aging at 473 K in the range of $0.4\,\mu$m, whereas aging at 338 K resulted in crystallites smaller than $0.1\,\mu$m. We synthesized HTs with different platelet sizes and, after activation and extensive characterization, determined their catalytic performance. We also measured the activity of a HT catalyst prepared via ion exchange. In this paper, we present our results from these experiments, which not only support the above-mentioned model, but also give fundamental insight into the transformation of the HT structure during activation.

EXPERIMENTAL

HT Preparation

An aqueous solution (45 ml) of 0.1 mol of $Mg(NO_3)_2 \cdot 6H_2O$ and 0.05 mol of $Al(NO_3)_3 \cdot 9H_2O$ was added all at once to a second solution (70 ml) containing 0.35 mol of NaOH and 0.09 mol of Na_2CO_3 at 333 K. The mixture was kept at this temperature for 1 h under stirring, after which the white precipitate was poured into a Teflon holder and placed into a stainless-steel rotating autoclave. After a 24-h crystallization and aging period (at 373, 423, and 473 K, respectively), the white precipitate was filtered and washed several times. The HT was dried for 24 h at 393 K. This resulted in the as-synthesized samples, designated as, e.g., $HT423_{as}$. All other samples have been denoted with the synthesis temperature and stage of activation, e.g., $HT423_{calc}$ and $HT423_{rehydr}$.

After drying, the HT was heated in a nitrogen flow up to 723 K with a heating rate of 10 K/min and kept at that temperature for 8 h. Samples (typically 0.5 g) were rehydrated at 313 K by use of a decarbonated water-saturated nitrogen flow (0.1 v/v) of 100 ml/min for 24 h. The rehydration procedure has been slightly modified from that of Rao *et al.* (1).

The HT with oxalate as compensating anion (denoted HT_{ox}) was synthesized using the procedure of Titulaer (30). An aqueous solution (25 ml) of 0.04 mol of $MgCl_2 \cdot 6H_2O$ and 0.02 mol of $AlCl_3 \cdot 6H_2O$ was added all at once to a second solution (66 ml) containing 6.3 mmol of $C_2H_2O_4 \cdot 2H_2O$ and 0.13 mol of KOH under nitrogen atmosphere. All solutions were previously boiled and outgassed to remove carbon dioxide from the solution. The mixture was stirred at 293 K for 90 min, after which a third solution (66 ml) containing 0.02 mol of $C_2H_2O_4 \cdot 2H_2O$ and 0.04 mol of KOH was added. The resulting solution was stirred at 367 K for 20 h. The resulting white precipitate was filtered and washed several times. The HT_{ox} was dried for 24 h at 333 K under nitrogen atmosphere.

Ion exchange of the HT_{ox} was achieved by addition of 1.0 g of HT_{ox} to a decarbonated 0.5 M KOH solution and stirring at reflux temperature under nitrogen atmosphere for at least 20 h. After washing and filtration, the ion-exchanged HT (HT_{ex}) was dried and stored under nitrogen.

Characterization

Powder X-ray diffaction (XRD) patterns were obtained by using an Enraf Nonius FR 590 with Co$K\alpha$ radiation. A Micromeritics ASAP 2400 analyzer was used for N_2 physisorption to determine surface areas and pore volumes. When micropores were present, the surface area S_T calculated with the *t*-method (surface area in pores > 2 nm) is reported instead of the BET surface area (31 and references therein). Volumetric CO_2 adsorption measurements in the pressure range 0–1 mbar were performed at 273 K using a Micromeritics ASAP 2000. Calcined and rehydrated calcined samples were stored under nitrogen to avoid CO_2 uptake from the atmosphere. Before characterization measurements were performed, the samples were outgassed under vacuum at 393 K. TEM images were obtained with a Philips CM-10 transmission electron microscope. A Philips XL-30 field emission gun (FEG) scanning electron microscope was used to obtain SEM images. ICP analysis was performed using a Perkin Elmer ICP-OES Optima 3000.

Reaction Procedures

The self-condensation reaction of acetone was performed in a stirred double-walled thermostatically cooled glass reactor, equipped with baffles. Typically, 116 g (2 mol)

of acetone was cooled to 273 K, and 0.3 g of freshly activated catalyst was added under a flow of nitrogen to exclude atmospheric carbon dioxide. Aliquots of 1 ml were taken from the reaction mixture during the 24-h reaction period and analyzed using a Chrompack CP 9001 GC provided with a Chrompack CP 9050 autosampler. Iso-octane (Merck) was used as an internal standard to calculate the amount of DAA formed.

RESULTS

The Mg/Al ratios from ICP analyses were close to the calculated synthesis values (Table 1), although with increasing synthesis temperature a slight increase toward the natural 3/1 distribution is observed as earlier reported by Vucelic *et al.* (33). Moreover, EDAX line scans showed a homogeneous distribution of Mg and Al in a ratio of 2 across the platelets. The XRD patterns as shown in Fig. 2 of HT423 after the different stages of activation are representative of the obtained results with all samples. The $HT423_{as}$ compound exhibits the typical features of a highly crystalline hydrotalcite material (4). We observed an increase in crystallinity with higher synthesis temperatures. The BET surface areas as well as the total pore volumes of the HT compounds show a decrease with increasing aging temperature. This is indicative of larger platelet sizes, since the total pore volume depends on surface area and pore diameter and the latter remained constant for the three hydrothermally synthesized samples (Table 1). In none of the samples were micropores present. The XRD patterns of the HT_{ox} and the HT_{ex} samples are also depicted in Fig. 2. The presence of oxalate in the interlayer gives rise to a 003 reflection at 9.8 Å ($2\Theta = 10.6$), which is in close agreement with values reported in literature (30, 32). The peak at 4.6 Å ($2\Theta = 22.7$, denoted with $*$ in Fig. 2) cannot be assigned straightforwardly on the basis of the HT structure. Vucelic *et al*. reported the same reflection in a HT (Mg/Al = 2) with interlayer benzoate (33). Similar observations were made by Gastuche *et al*. (4, 34) and Serna *et al*. (35), which they ascribed to a superlattice in the *ab*-plane of the HT, indicating a high degree of cation ordering. Bookin *et al*. demonstrated that only a single superlattice reflection from interlayer ordering can be expected (36). The XRD patterns of HT_{ox} and HT_{ex} in Fig. 2 demonstrate that the exchange of oxalate with OH^- had been successful. The 003 reflection shifted from 9.8 Å to 7.7 Å ($2\Theta = 13.9$), with no 003 reflection of HT_{ox} remaining. SEM images of $HT423_{as}$ (Fig. 3a) and $HT473_{as}$ (Fig. 3b) emphasize the difference in lateral platelet sizes due to the synthesis temperatures. TEM micrographs show regular hexagonally shaped structures. Figure 4a depicts $HT423_{as}$ crystallites with top and side views from which the HT crystallite stack thickness can be derived. The determined lateral platelet sizes in Table 1 are in close agreement with those reported by Reichle *et al.* (29).

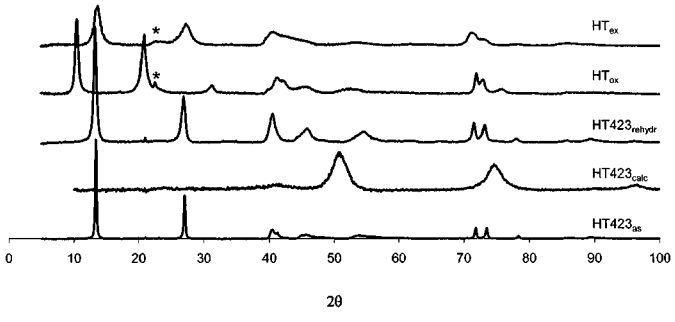

FIG. 2. XRD patterns of hydrotalcite with interlayer carbonate synthesized at 423 K ($HT423_{as}$); after calcination at 723 K ($HT423_{calc}$); after calcination/rehydration ($HT423_{rehydr}$); hydrotalcite with interlayer oxalate (HT_{ox}) and HT_{ox} after ion exchange with KOH (HT_{ex}). $*$ indicates superlattice reflection.

TABLE 1

Results from Physisorption and Characterization Measurements: Samples as Synthesized

	Mg/Al[a]	S_{BET} (m^2/g)	Micropore volume (ml/g)	Total pore volume (ml/g)	Platelet size (nm)[b]	Pore diameter (nm)[c]
$HT\ 373_{as}$	2.2	67	0.00	0.49	50	29
$HT\ 423_{as}$	2.3	35	0.00	0.26	150	30
$HT\ 473_{as}$	2.5	17	0.00	0.11	430	26
HT_{ox}	2.2	56	0.00	0.53	110	38

[a] ICP analysis.
[b] Lateral dimension, determined using TEM.
[c] Cylindrical pore diameter (PD); PD = 4000 × pore volume/S_{BET}.

Calcination of the HT materials up to 723 K resulted in the disappearance of the layered structure as can be concluded from the absence of the 00*l* signals in the XRD pattern of $HT423_{calc}$ shown in Fig. 2. Due to dehydroxylation and interlayer carbonate decomposition, water and carbon dioxide are released, giving rise to an increased mesopore volume (compared to that of the as-synthesized samples) and formation of micropores (29), which results in high BET values. When micropores are present, it is more appropriate to use the external surface areas calculated from the *t*-plot (31 and references therein). These values are given for the three calcined samples in Table 2. The crystallite size difference due to the aging temperature is preserved after calcination, since the decrease in total pore volume as well as (*t*-plot) surface area occurs also with these samples. Indeed, the TEM image of $HT423_{calc}$ in Fig. 4b shows that the morphology of the crystallites had largely been retained. The corresponding XRD pattern of $HT423_{calc}$ in Fig. 2 shows broad signals, which can be attributed to MgO. The larger the crystallites before calcination, the higher the micropore volume after calcination due to increased water and CO_2 evolution.

Rehydration of the samples calcined at 723 K resulted in the reconstruction of the layered structure, due to the HT

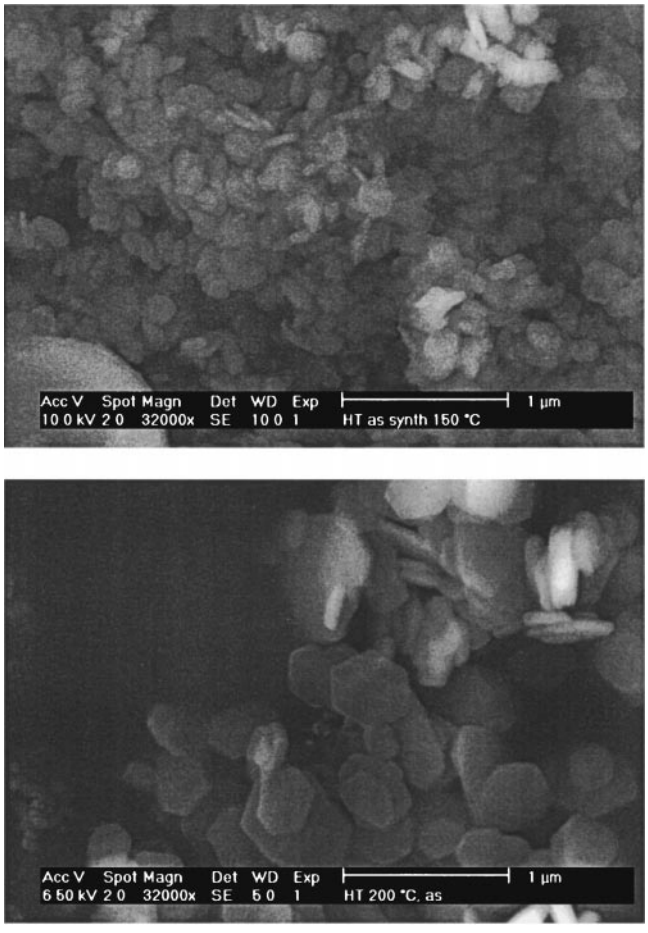

FIG. 3. SEM images of (a, top) hydrotalcite synthesized at 423 K ($HT423_{as}$); (b, bottom) hydrotalcite synthesized at 473 K ($HT473_{as}$).

"memory effect," the characteristic feature of this mixed oxide to be transformed back to the HT structure ($HT423_{rehydr}$ in Fig. 2), although peak broadening as compared with the non-calcined samples and loss of crystallinity are apparent (4, 37). Earlier XANES results showed that the rehydration treatment as executed here entirely restored the original Al^{3+} and Mg^{2+} coordinations up to a distance of 15 Å, the maximum distance at which XAFS spectroscopy is sensitive (18). This observation deviates from that of other studies (38, 39), in which it was concluded that part of the Al^{3+} ions remains tetrahedrally coordinated after rehydration. Possible explanations for these different results might be an incomplete reconstruction upon rehydration due to the lower water vapor pressure used in these studies or the different duration of the rehydration periods. Nevertheless, if sufficient time is taken and the calcination temperature has not exceeded 723 K, a complete repair of the original Al^{3+} coordination can be achieved. ^{27}Al-MAS-NMR data from Rey *et al.* show results similar to ours (40). The mesopores created by calcination retained after rehydration, whereas the micropores disappeared (Table 2). The pore volume of the $HT373_{rehydr}$ was somewhat lower than expected in view of the crystallite size difference as observed for the as-synthesized and the calcined samples. However, clear differences can be observed in the mesopore size distributions of samples before and after calcination/rehydration (Fig. 5). The activation resulted in the formation of smaller mesopores (~8 nm). The TEM images of $HT423_{rehydr}$ and $HT473_{rehydr}$ (Figs. 6a and 6b) show the effect of rehydration: a morphology completely different from that of the original HT structure. The regular stacks of hexagonal platelets still present after calcination have been transformed into an irregular but layered HT structure, giving the XRD pattern shown in Fig. 2. The smaller mesopores probably originate from spaces within the crystallite agglomerates created by calcination/rehydration. In most studies catalysts have been synthesized at a temperature below 373 K (1–3, 13, 23) in order to obtain small crystallites and then these differences in morphology are not easily recognized.

The pore size distribution of HT_{ex} differs from that of HT_{ox} (Fig. 7), as the average pore diameter was lowered.

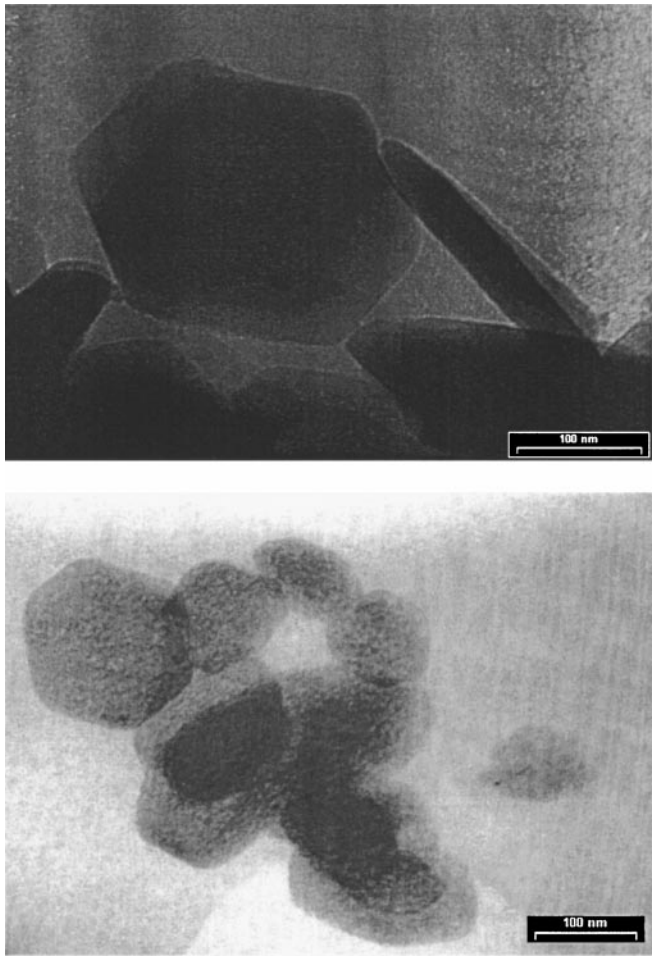

FIG. 4. TEM images of (a, top) hydrotalcite synthesized at 423 K ($HT423_{as}$); (b, bottom) hydrotalcite synthesized at 423 K after calcination ($HT423_{calc}$).

TABLE 2

Results from Physisorption and Characterization Measurements

	Surface area (m^2/g)[a]	Micropore volume (ml/g)	Total pore volume (ml/g)	CO_2 uptake (ml STP CO_2/g)	CO_2/Al (mol%)[b]
$HT373_{calc}$	120*	0.03	0.66	n.d.	n.d.
$HT423_{calc}$	80*	0.04	0.42	n.d.	n.d.
$HT473_{calc}$	40*	0.07	0.20	n.d.	n.d.
$HT373_{rehydr}$	79	0.00	0.27	3.0	3.7
$HT423_{rehydr}$	67	0.00	0.39	1.6	1.9
$HT473_{rehydr}$	37	0.00	0.27	1.2	1.5
HT_{ex}	64	0.00	0.47	7.5	9.3

[a] BET surface area or, when marked with ∗, surface area calculated with *t*-method.

[b] Moles of adsorbed CO_2 per moles of Al present in HT, calculated from ICP analysis.

This is probably due to a slightly different intercrystallite packing brought about by the ion exchange procedure. More importantly, the ion exchange did not result in the formation of mesopores of about 8 nm as with the calcination/rehydration procedure. Furthermore, a TEM image of HT_{ex} shows that ion exchange did not alter the hexagonal structure either (Fig. 8).

CO_2 adsorption at low pressures has been used to determine the amount of accessible basic sites (2, 41). From the results in Table 2 it appears that CO_2 adsorpion under the prevailing conditions is restricted to a minor part (1–4%) of the Al^{3+}–OH^- sites. Since every interlayer OH^- inevitably coincides with an Al^{3+} ion in the rehydrated HT structure, this is remarkable. We have previously proposed a model in which the CO_2 uptake is limited to OH^- ions present at or near edges of the platelets (2). The CO_2 uptake shows an increase with decreasing aging temperature, indicating that the difference in the original platelet sizes has an impact on the activated samples.

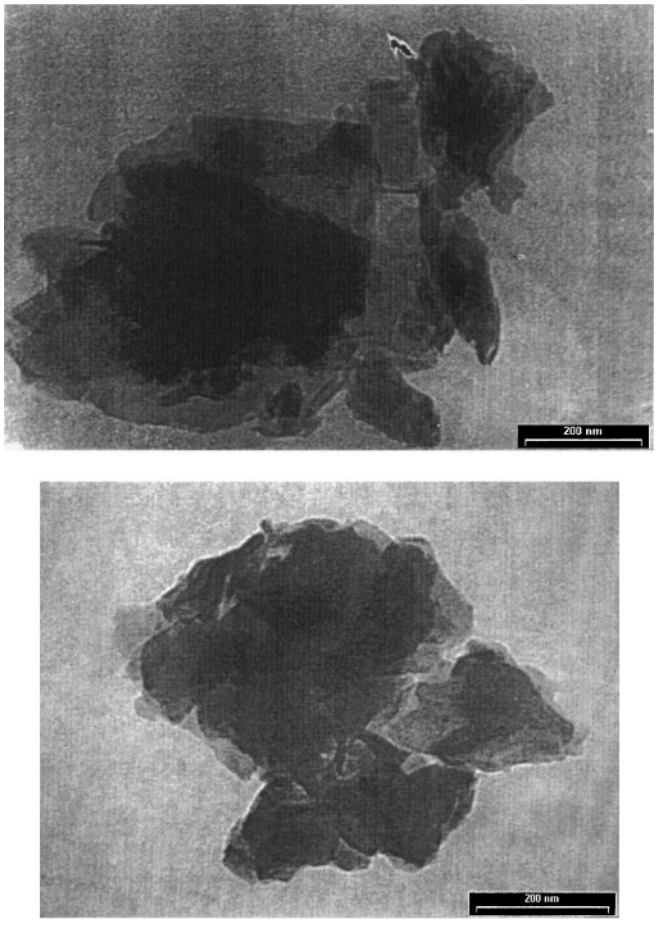

FIG. 6. TEM images of (a, top) hydrotalcite synthesized at 473 K after calcination/rehydration ($HT473_{rehydr}$); (b, bottom) hydrotalcite synthesized at 423 K after calcination/rehydration ($HT423_{rehydr}$).

Figure 9 depicts the catalytic performances in the self-condensation of acetone of the activated HTs with different platelet sizes and of HT_{ex}. Clearly, the larger the original

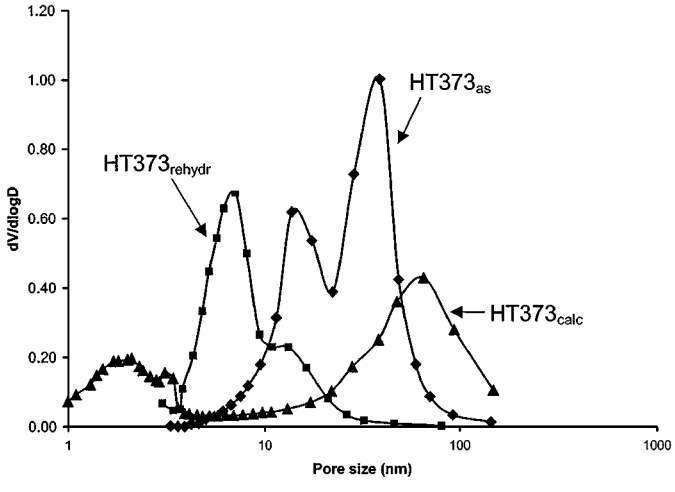

FIG. 5. Pore size distributions of hydrotalcite synthesized at 373 K ($HT373_{as}$); after calcination at 723 K ($HT373_{calc}$); after calcination/rehydration ($HT373_{rehydr}$).

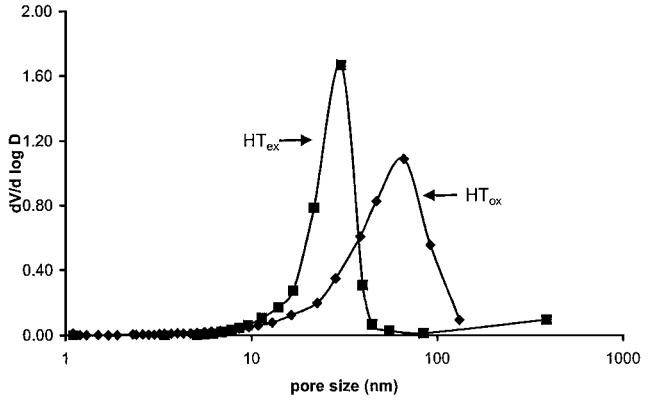

FIG. 7. Pore size distributions of hydrotalcite with interlayer oxalate (HT_{ox}) and HT_{ox} after ion exchange with KOH (HT_{ex}).

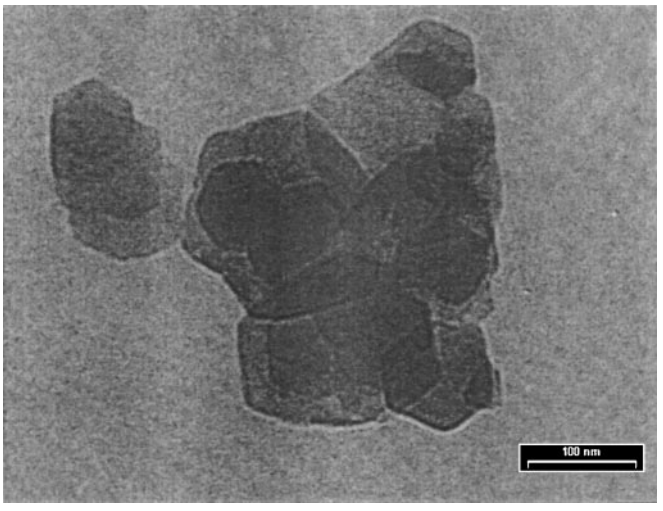

FIG. 8. TEM image of hydrotalcite after ion exchange with KOH (HT_{ex}).

platelet size, the lower the obtained activity. Dehydration of DAA to mesityl oxide (MO) was not observed at 273 K. The catalytic activity of HT_{ex} is low but significant. Its initial activity was 0.6 $g_{DAA}\ g_{cat}^{-1}\ h^{-1}$, which is 20 times lower than the initial activity of $HT373_{rehydr}$. Figure 10 shows the initial activities of the samples versus the number of sites as measured by CO_2 adsorption. A linear correlation of the initial activity of activated HTs with different platelet sizes and the adsorption of CO_2 was observed. Surprisingly, the CO_2 adsorption of HT_{ex} (and with this the number of accessible sites) is very high when compared with those of $HT373_{rehydr}$, $HT423_{rehydr}$, and $HT473_{rehydr}$. A calculation based on the hexagonal geometry indicates that the amount of adsorbed CO_2 with HT_{ex} correlates well with the exposed edge area on the stacked platelets.

DISCUSSION

In general the activation of HTs via thermal treatment and rehydration is considered to involve the replacement of interlayer carbonate by hydroxyl ions without a drastic effect on the original ordered stacked structure of the aggregates. Earlier work from our group (2) resulted in the proposed model as shown in Fig. 11. Of the introduced and required OH^- anions in the interlayer via calcination/rehydration, only a minor part partakes in the base-catalyzed aldol condensation. From Table 2 (last column) it is clear that the participating number of basic sites (of calcined/rehydrated samples) does not exceed 5%.

The synthesis of HTs with different platelet sizes by variation of the aging temperature was successful. Platelet sizes varying in the range of 50–430 nm were obtained. After activation, the sequence in the original platelet sizes is retained in the samples, as can be concluded from the increase of the number of basic sites with decreasing synthesis temperature (Table 2). Furthermore, a decrease in initial activity can be seen with increasing platelet size and decreasing BET surface area. This is in itself remarkable in view of the total lattice disintegration upon calcination. The initial activities in the self-condensation of acetone corresponded well with the measured number of sites of the calcined/rehydrated samples (Fig. 10). Both results support the model in which the condensation reaction proceeds at Brønsted basic sites near the edges of HT platelets, as depicted in Fig. 11.

Our results show that activation implies more than solely the introduction of the required basic OH^- sites. Although the presence of these hydroxyl ions is a prerequisite, high activities are obtained only after calcination/rehydration, i.e., after disordering of the original structure. The effects of our two distinct activation procedures are schematically drawn in Fig. 12. In the case of ion exchange, the original HT

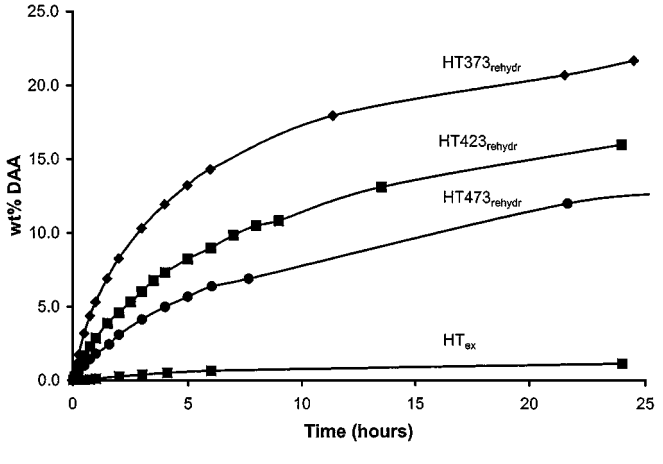

FIG. 9. DAA production at 273 K of via calcination/rehydration activated hydrotalcites synthesized at 373 K ($HT373_{rehydr}$ (▲)), 423 K ($HT423_{rehydr}$ (◆)), 473 K ($HT473_{rehydr}$ (●)), and activated via ion exchange with KOH (HT_{ex} (■)).

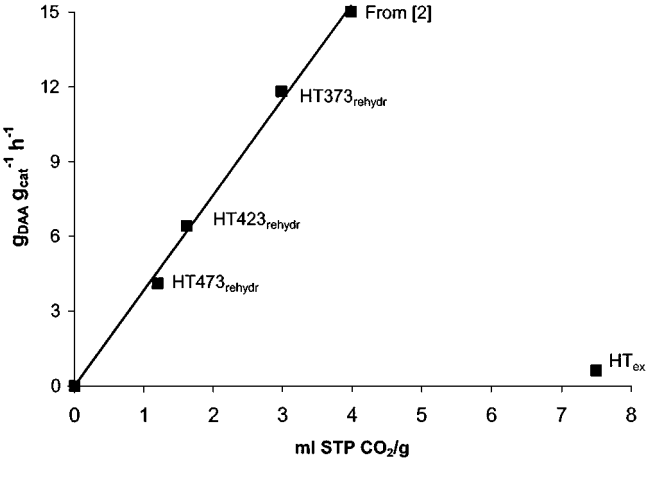

FIG. 10. Relation between initial activity and CO_2 adsorption of via calcination/rehydration activated hydrotalcites synthesized at 373 K ($HT373_{rehydr}$), 423 K ($HT423_{rehydr}$), 473 K ($HT473_{rehydr}$), and activated via ion exchange with KOH (HT_{ex}).

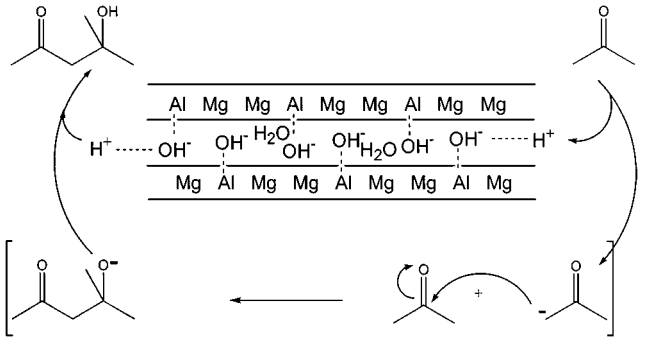

FIG. 11. Proposed catalytic mechanism of aldol condensation for the self-condensation of acetone at basic sites between edges of HT platelets (2).

structure is largely retained, whereas calcination/rehydration results in transformation of the ordered HT structure into an irregular one (Figs. 6 and 8) and formation of mesopores of about 8 nm (Fig. 5). These mesopores probably originate from spaces within the aggregates. Presumably, calcination/rehydration results in platelets that are randomly aggregated [similar to the morphology of smectites (42)] as shown in Fig. 12.

That the morphology is an important factor affecting the catalytic activity is demonstrated by the striking difference in catalytic performance as well as in CO_2 adsorption of the thermally activated samples and the sample activated by ion exchange (Fig. 9 and Table 2, respectively). If only the amount of basic sites determined the activity, an initial activity about 50 times higher should have been measured with the ion-exchanged sample. More precisely, from the extrapolated correlation between the initial activities of the thermally activated samples (Fig. 10) we would have expected an initial activity of 29 $g_{DAA}\ g_{cat}^{-1}\ h_{ini}^{-1}$ with the exchanged sample. We measured an initial activity as low as 0.6 $g_{DAA}\ g_{cat}^{-1}\ h^{-1}$. Expressed in TOFs: 5 h_{ini}^{-1} for HT_{ex} and around 200 h_{ini}^{-1} for the calcined/rehydrated samples. This difference can only be explained by a significant difference in basic strength of the OH^- ions, those in the exchanged HT being weaker than those in the thermally activated HTs. Apparently, the less regular structure brings along an increase in basic strength and, due to this, an enhanced catalytic activity. Future work is advocated involving direct measurement of basic strength in these catalysts.

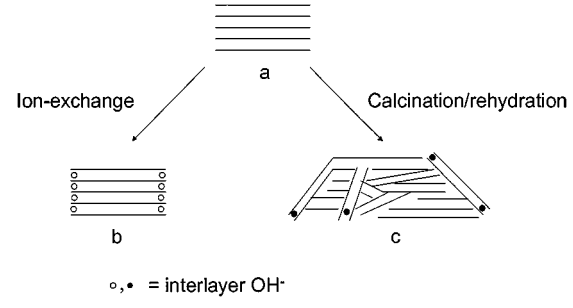

FIG. 12. Effect of activation treatment on HT structure: (a) HT as synthesized; (b) HT after ion exchange; (c) HT structure after calcination/rehydration.

Many authors used the thermal route to replace carbonate for other ions, e.g., organic anions (43) and polyoxometalates (POMs) (24) in the HT. Our results demonstrate that phenomena ascribed to these interlayer anions probably are also connected with the change in structure of the HT.

CONCLUSION

Besides incorporation of OH^- as an interlayer anion, thermal activation and rehydration of the precursor HT-CO_3 gives rise to the formation of irregular aggregates containing mesopores of around 8 nm. These changes result in a higher basicity of OH^- near the edges of HT platelets, which is essential to obtain a highly active HT catalyst for liquid-phase aldol condensation reactions.

ACKNOWLEDGMENTS

Financial support from the Innovation Oriented Research Programmes (IOP Catalysis), an initiative of the Dutch Ministry of Economic Affairs, is gratefully acknowledged. Furthermore, we thank Marjan Versluijs-Helder (SEM) and John Raaymakers (physisorption) for their technical assistance.

REFERENCES

1. Rao, K. K., Gravelle, M., Valente, J., and Figueras, F., *J. Catal.* **173**, 115 (1998).
2. Roelofs, J. C. A. A., Van Dillen, A. J., and De Jong, K. P., *Catal. Today* **60**, 297 (2000).
3. Roelofs, J. C. A. A., Van Dillen, A. J., and De Jong, K. P., *Catal. Lett.* **74**, 91 (2001).
4. Cavani, F., Trifiro, F., and Vaccari, A., *Catal. Today* **11**, 173 (1991).
5. Van der Pol, A., Mojet, B. L., Van der Ven, E., and De Boer, E., *J. Phys. Chem.* **98**, 4050 (1994).
6. Kagunya, W., Dutta, P., and Lei, Z., *Physica B* **234**, 910 (1997).
7. Reichle, W. T., *J. Catal.* **63**, 295 (1980).
8. Suzuki, E., and Ono, Y., *Bull. Chem. Soc. Jpn.* **61**, 1008 (1988).
9. Corma, A., and Martin-Aranda, R., *Appl. Catal.* **105**, 271 (1993).
10. Climent, M. J., Corma, A., Iborra, S., and Primo, J., *J. Catal.* **151**, 60 (1995).
11. Constantino, V. R. L., and Pinnavaia, T. J., *Catal. Lett.* **23**, 361 (1994).
12. Di Cosimo, J. I., Diez, V. K., Xu, M., Iglesia, E., and Apesteguia, C. R., *J. Catal.* **178**, 499 (1998).
13. Guida, A., Hassane Lhouty, M., Tichit, D., Figueras, F., and Geneste, P., *Appl. Catal.* **164**, 251 (1997).
14. Tichit, D., Naciri Bennani, M., Figueras, F., Tessier, R., and Kervennal, J., *Appl. Clay Sci.* **13**, 401 (1998).
15. Miyata, S., *Clays Clay Miner.* **28**, 50 (1980).
16. Hudson, M. J., Carlino, S., and Apperley, D. C., *J. Mater. Chem.* **5**, 323 (1995).
17. Belotto, M., Rebours, B., Clause, O., and Lynch, J., *J. Phys. Chem.* **100**, 8535 (1996).
18. Van Bokhoven, J. A., Roelofs, J. C. A. A., De Jong, K. P., and Koningsberger, D. C., *Chem. Eur. J.* **6**, 1258 (2001).
19. Lippert, S., Baumann, W., and Thomke, K., *J. Mol. Catal.* **69**, 199 (1991).

20. Podrebarac, G., Ng, F., and Rempel, G., *Chem. Eng. Sci.* **52**, 2991 (1997).
21. Salvapati, G., Ramanamurty, K., and Janardanarao, M., *J. Mol. Catal.* **54**, 9 (1989).
22. Craven, E., *J. Appl. Chem.* **13**, 71 (1963).
23. Prinetto, F., Tichit, D., Teissier, R., and Coq, B., *Catal. Today* **55**, 103 (2000).
24. Newman, S. P., and Jones, W., *New J. Chem.* 105 (1998).
25. Carlino, S., *Solid State Ionics* **98**, 73 (1997).
26. Miyata, S., *Clays Clay Miner.* **31**, 305 (1983).
27. Israëli, Y., Taviot-Guého, C., Besse, J.-P., Morel, J.-P., and Morel-Desrosiers, N., *J. Chem. Soc., Dalton Trans.* 791 (2000).
28. Kaneyoshi, M., and Jones, W., *Chem. Phys. Lett.* **296**, 183 (1998).
29. Reichle, W. T., Kang, S., and Everhardt, D. S., *J. Catal.* **101**, 352 (1986).
30. Titulaer, M. K., Ph.D thesis, Utrecht University, 1993.
31. Van Santen, R. A., Van Leeuwen, P. W. N. M., Moulijn, J. A., and Averill, B. A., "Catalysis: an Integrated Approach." Elsevier, Amsterdam, 1999.
32. Miyata, S., and Kumura, T., *Chem. Lett.* 843 (1973).
33. Vucelic, M., Moggridge, G. D., and Jones, W., *J. Phys. Chem.* **99**, 8328 (1995).
34. Gastuche, M. C., Brown, G., and Mortland, M. M., *Clay Miner.* **7**, 177 (1967).
35. Serna, C. J., Rendon, J. L., and Iglesias, J. E., *Clays Clay Miner.* **30**, 180 (1982).
36. Bookin, A. S., Cherkashin, V. I., and Drits, V. I., *Clays Clay Miner.* **41**, 558 (1993).
37. Miyata, S., *Clays Clay Miner.* **28**, 50 (1980).
38. Rocha, J., Del Arco, M., Rives, V., and Ulibarri, M. A., *J. Mater. Chem.* **9**, 2499 (1999).
39. Beres, A., Palenko, I., Bertrand, J. C., Nagy, J. B., and Kiricsi, I., *J. Mol. Struct.* **13**, 410 (1997).
40. Rey, F., Fornes, V., and Rojo, J. M., *J. Chem. Soc., Faraday Trans.* **88**, 2233 (1992).
41. Sanchez Valente, J., Figueras, F., Gravelle, M., Kumbhar, P., Lopez, J., and Besse, J.-P., *J.Catal.* **189**, 370 (2000).
42. Vogels, R. J. M. J., Ph.D thesis, Utrecht University, 1996.
43. Chibwe, K., and Jones, W., *J. Chem. Soc., Chem. Commun.* 926 (1989).